IEEE Photonics Journal
An IEEE Photonics Society Publication

Open Access

Photonics-Assisted Broadband Distributed Coherent Aperture Radar for High-Precision Imaging of Dim-Small Targets

Volume 11, Number 5, October 2019

Xuedi Xiao
Shangyuan Li
Xiaoxiao Xue
Luhang Xing
Shaowen Peng
Xiaoping Zheng
Bingkun Zhou

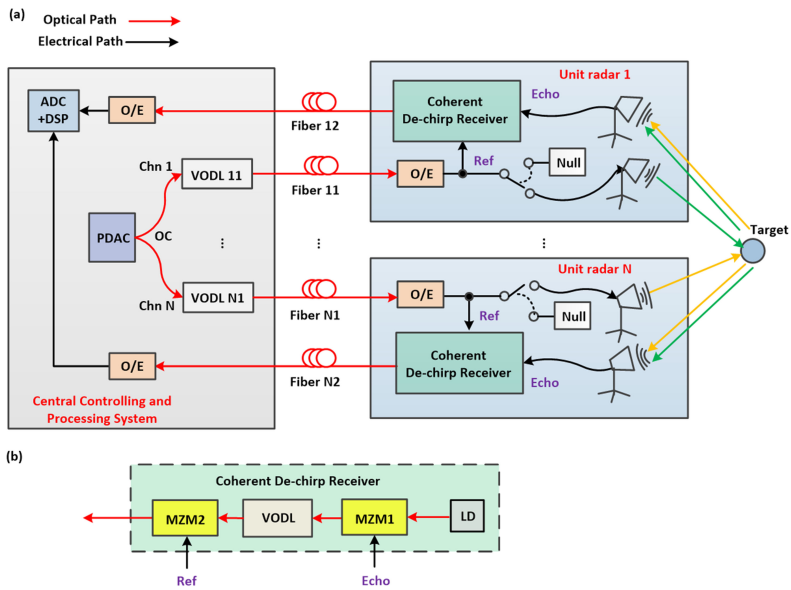

DOI: 10.1109/JPHOT.2019.2934472

Photonics-Assisted Broadband Distributed Coherent Aperture Radar for High-Precision Imaging of Dim-Small Targets

Xuedi Xiao, Shangyuan Li, Xiaoxiao Xue, Luhang Xing, Shaowen Peng, Xiaoping Zheng, and Bingkun Zhou

The authors are with the Beijing National Research Center for Information Science and Technology, Department of Electronic Engineering, Tsinghua University, Beijing 100084, China

DOI:10.1109/JPHOT.2019.2934472

Manuscript received June 14, 2019; revised July 14, 2019; accepted August 7, 2019. Date of publication August 12, 2019; date of current version August 23, 2019. This work was supported in part by the National Nature Science Foundation of China under Grants 61690191, 61690192, 61420106003, and 61621064, in part by the Beijing Natural Science Foundation under Grant 4172029, and in part by the Chuanxin Funding. Corresponding author: Xiaoping Zheng (e-mail: xpzheng@mail.tsinghua.edu.cn).

Abstract: High-precision imaging of dim-small target is demonstrated using a photonics-assisted broadband distributed coherent aperture radar (DCAR). The photonics-based methods lead to a high resolution, making it possible to discriminate small targets. In addition, the cooperative work of multiple radars enhances the signal-to-noise ratio (SNR) and helps to improve the imaging precision. Experimentally, the inverse synthetic aperture radar (ISAR) coherent imaging for a small unmanned aerial vehicle is conducted by a two-unit X-band DCAR (8–12 GHz), and the range and cross-range resolution are ∼3.4 cm and ∼3.6 cm, respectively. About 8.5 dB image SNR gain can be achieved in full-coherence mode compared to that in monostatic mode. Taking advantage of the SNR gain, the scatters that are below the noise floor when in monostatic mode can be clearly seen when full-coherence is realized, which reveals that the proposed photonics-assisted DCAR improves the imaging precision and makes it easier to identify dim-small targets.

Index Terms: Distributed coherent aperture radar, microwave photonics, dim-small targets, imaging.

1. Introduction

High-Precision detection and imaging of dim-small targets are crucial issues in both military and civil areas. It has aroused attention worldwide in many applications such as anti-stealth technique, safety navigation, and ocean environment monitoring [1]–[4]. To realize imaging and identification of small targets, the radar systems with high resolution are required, which corresponds to wideband waveform generation and processing. In addition, high signal-to-noise ratio (SNR) would help to enhance the detection and imaging precision [5]. However, the echo wave of dim-small target is very weak and usually overwhelmed by noise due to the small radar cross section (RCS), yields low SNR and deteriorated detection performance [6]. To overcome this issue, the radar systems with improved

transmitted power, antenna aperture and antenna gain can be applied, which are expensive to build and difficult to transport [5]. The distributed coherent aperture radar (DCAR) offers a viable approach to cope with the above dilemma [7], [8]. In such radar system, N geographically distributed small-aperture unit radars radiate radar signals to the same target and realize the coherent syntheses of these signals with the control of the central controlling and processing system. When full-coherence is obtained, an SNR gain of N^3 can be obtained over a unit radar, improving the detection precision. As each unit radar has a small aperture, the DCAR can be easier to build and transport than the radars with large apertures [8]. Recently, several DCAR systems have been established, and coherence syntheses on the stationary and moving targets are implemented, verifying the feasibility of the DCAR concept [7]–[11]. The above presented DCARs all show the ability to enhance the SNR, which will help to improve the detection precision. Nevertheless, range resolution of these systems are limited up to decimeter-level, which restricts the capability to image and discriminate small targets. And it's difficult to further broaden the bandwidth because of the limitation of electronic devices, for example the large time jitter introduced by the direct digital synthesizers and analog to digital converters (ADCs) [12], [13]. Thus high-precision imaging of dim-small targets is still challenging.

Recently, microwave photonics has been considered to have the potential to deal with these challenges, thanks to its advantages of ultra-wide bandwidth, ultra-low transmission loss, flexible reconfiguration and immunity to electromagnetic interference [14], [15]. In [16]–[20], the photonics-based monostatic high-resolution imaging radar systems have been intensively studied. Wideband radar signals are generated and processed through photonic-assisted methods, making it capable to get detailed information from the high-resolution images of the targets. Nevertheless, the echo wave SNR is still restricted by the transmitted power of the single transmitter. In [21], we have demonstrated a photonics-assisted wideband DCAR. The wideband radar waveforms are generated through optical methods, and the echo waves are directly sampled by the ADC. Finally, by digitally compensating the delay and phase differences between the echo waves of different receivers and adding the compensated results, receive coherence is implemented. The coherent synthesis for a static metal ball is demonstrated, and an 8.3 dB SNR gain is obtained by a two-unit DCAR. The direct sampling method puts great pressure on the ADC and causes great data volume. The further digital compensation also leads to a large amount of computation and a long processing time. And realizing moving target imaging by accumulating multiple pulse periods will exacerbate these problems. Therefore realizing the coherent imaging of dim-small moving targets and improving the identification precision remain a problem.

In this paper, we improve the receiver and establish a photonics-assisted broadband DCAR for high-precision imaging of dim-small targets. The improved coherent de-chirp receiver is based on the cascaded Mach-Zehnder modulators (MZMs) and the variable optical delay line (VODL). The de-chirp processing significantly lowers the speed of the ADC and reduces the data bulk [22]. Meanwhile, time delay of the echo wave can be precisely adjusted by the VODL to promote the coherent receiving between different receivers, which helps to omit digital time delay compensation and reduce the computation load. Combining with the wideband linear frequency modulated waveform (LFMW) generation by the photonic digital-to-analog converter (PDAC), a high imaging resolution can be acquired by the DCAR, making it possible to recognize small targets. Besides, the image SNR can be enhanced as multiple unit radars work collaboratively, which improves the imaging precision and makes it easier to identify dim-small targets. Experimentally, the inverse synthetic aperture radar (ISAR) coherent imaging experiment for a small unmanned aerial vehicle (UAV, 0.3 m $\times$ 0.3 m) is carried out by a two-unit X-band DCAR (8–12 GHz). The range and cross-range resolution are $\sim$3.4 cm and $\sim$3.6 cm. When full-coherence is realized, about 8.5 dB image SNR gain can be obtained compared to that in monostatic mode. Due to the SNR gain, the target scatters that are submerged in noise when in monostatic mode can be clearly seen when full-coherence is realized. Put another way, the system improves the SNR and makes it easier to identify dim-small moving targets.

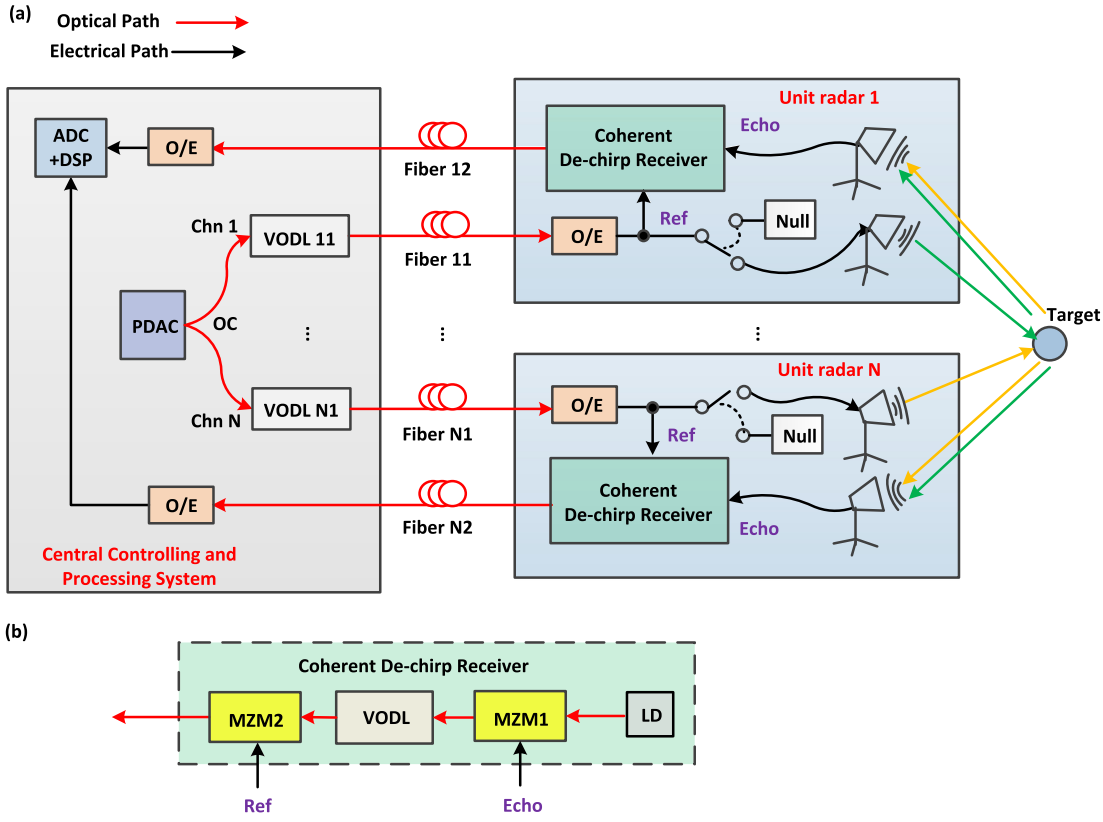

Fig. 1. (a) Configuration of the photonic-assisted broadband DCAR; DSP: digital signal processor. PDAC: photonic digital-to-analog converter; O/E: optical/electrical; OC: optical coupler; VODL: variable optical delay line; (b) Configuration of the coherent de-chirp receiver; LD: laser diode; MZM: Mach-Zehnder modulator.

2. Operation Principle

Figure 1(a) demonstrates the configuration of the photonics-assisted broadband DCAR. The photonic digital-to-analog converter (PDAC) combined with the optical coupler (OC) generate N-channel optical-carried LFMWs in the central controlling and processing system [23]. Then the emission time of each optical signal is tuned by the following VODL. After that, the signal is transmitted to the unit radar in the optical fiber, converted into microwave LFMW by the optical/electrical (O/E) conversion module, and divided into two parts. One part is fed into a microwave switch, which controls that the LFMW is emitted into free space by the horn antenna or blocked. And another part drives the coherent de-chirp receiver as the reference signal of the de-chirp process. Figure 1(b) shows the configuration of the coherent de-chirp receiver. The reflected target echo firstly modulates the continuous lightwave from the laser diode (LD) in a Mach-Zehnder modulator (MZM1). Then the optical-carried echo is delayed via the VODL, and modulated by the reference signal in MZM2. Next, the output of MZM2 is transmitted back to the central controlling and processing system, and the de-chirp process of the echo wave is implemented through the frequency mixing between the reference signal and the echo wave in the O/E conversion module. Finally, the intermediate frequency (IF) signals are digitalized by the ADC, and processed in the digital signal processor (DSP).

The radar firstly estimates the one-way time delay between the i-th unit radar and the target, which is denoted as τ_i. To achieve the necessary distinction between the waveforms emitted by multiple unit radars, here we use time-division multiplexing (TDM), which means that only one LFMW is emitted into space at a time by controlling the microwave switches. Then the IF signal

obtained by the i-th de-chirp receiver can be written as

$$s_{iIF}(t) = \cos\left[4k\pi\tau_i t + 4\pi f_0\tau_i - 4k\pi\tau_i^2\right], \tag{1}$$

where k and f_0 stand for the chirp rate and initial frequency of the LFMW. And the time delay can be figured out through the fast Fourier transform (FFT) of the IF signal.

Next, the radar operates in transmit-coherence mode, when all the LFMWs are emitted to the space at a time. On the basis of the estimated time delays, emission times of the waveforms are adjusted by the VODLs. And the transmit waveform of the i-th unit radar is $s'_{iT}(t) = s(t - \tau_b + \tau_i)$, where $s(t) = \cos(2\pi f_0 t + k\pi t^2)$, and τ_b is a basic time delay of each unit radar. Thus the superimposed waveform at the target is $S_{all}(t) = Ns(t - \tau_b)$, and the echo collected by the i-th unit radar will be $s'_{iR}(t) = Ns(t - \tau_b - \tau_i)$. Then the echo is converted into optical domain by MZM1 and time delayed by the following VODL. And the time delayed echo wave is $s''_{iR}(t) = Ns(t - \tau_b - \tau_i - \Delta\tau_{ir})$, where $\Delta\tau_{ir}$ is the time delay introduced by the VODL. Finally through the de-chirp process, the output IF signal will be

$$s'_{iIF}(t) = N\cos\left[2k\pi(2\tau_i + \Delta\tau_{ir})t + 2\pi f_0(2\tau_i + \Delta\tau_{ir}) - k\pi(2\tau_b + \Delta\tau_{ir})(2\tau_i + \Delta\tau_{ir})\right] \tag{2}$$

From Eqs. (1) and (2), we can infer that the peak power of the FFT result of the IF waveform is $G_s = N^2$ times that of the monostatic result (only one unit radar works). Meanwhile as the noise power is the same as one unit radar, the SNR gain is N^2, which will be $10\log N^2$ when the unit is dB.

From Eq. (2), we can also see that the de-chirped IF signals obtained by different receivers have different frequencies and phases without any compensations, and the following coherent receiving cannot be realized. Through digital signal processing, the phase differences can be compensated. While as for the frequency differences, a high sampling rate in frequency domain are needed to realize high-precision frequency compensation such as the methods of oversampling and digital interpolation, which will cause great computation load and long processing time. Here we use the high-precision VODL to tune the time delay of the echo wave, when we set $\Delta\tau_{ir} = 2\tau_b - 2\tau_i$, the output IF signal in Eq. (2) can be rewritten as

$$s'_{iIF}(t) = N\cos\left[4k\pi\tau_b t + 4\pi f_0\tau_b + 4k\pi\tau_b\tau_i - 8k\pi\tau_b^2\right] \tag{3}$$

which shows that the IF signals with the same frequency are obtained at all receivers and only the signal phases are different. Through simple digital signal processing, the phase differences can be figured out and compensated, thus the coherent receiving between different receivers can be obtained easily. The compensated IF signal is $s''_{iIF}(t) = N\cos(4k\pi\tau_b t)$. By adding them coherently, full-coherence is realized and the combined IF signal is

$$S_{all\_IF}(t) = \sum_{i=1}^{N} s''_{iIF}(t) = N^2\cos(4k\pi\tau_b t) \tag{4}$$

The results show that the peak power gain of the FFT result of the IF signal is $G_s = N^4$ compared to the monostatic result. As the noises in different receivers are independent, the noise power gain is $G_n = N$. Thus the SNR gain is N^3, which will be $10\log N^3$ when the unit is dB.

3. Experiment Results

Figure 2 demonstrates the detailed configuration of a two-unit DCAR, which is established to prove the feasibility of the proposed photonics-assisted system. A PDAC, an erbium-doped fiber amplifier (EDFA), and an OC generate two channels of the optical-carried LFMW in the central controlling and processing system. At each unit radar, the microwave LFMW (8–12 GHz) is generated after the optical-to-electrical conversion in a photodetector (PD), amplification by an electrical amplifier (EA), and filtering by a band-pass filter (BPF, 8–12 GHz). Then a power splitter (PS) splits the microwave LFMW into two branches. One part is fed into a microwave switch, and another part is sent to the cascaded MZMs-based coherent de-chirp receiver as the reference signal. To imitate

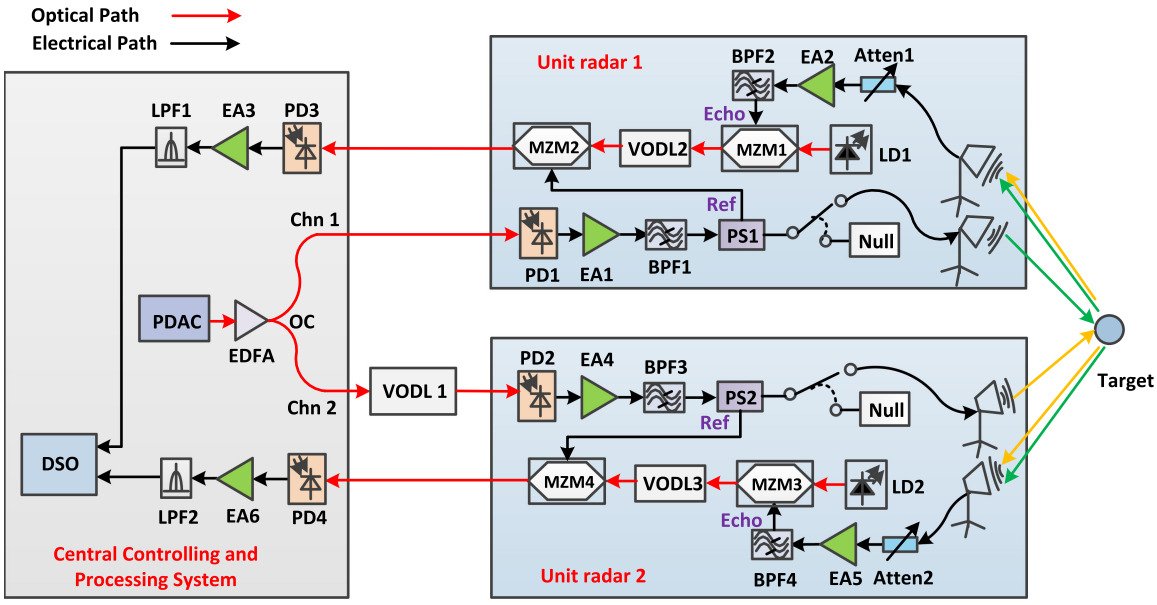

Fig. 2. Detailed experimental configuration of the proposed DCAR. DSO: digital signal oscilloscope; LPF: low-pass filter; EA: electrical amplifier; PD: photodetector; EDFA: erbium-doped fiber amplifier; BPF: band-pass filter; PS: power splitter; Atten: attenuator.

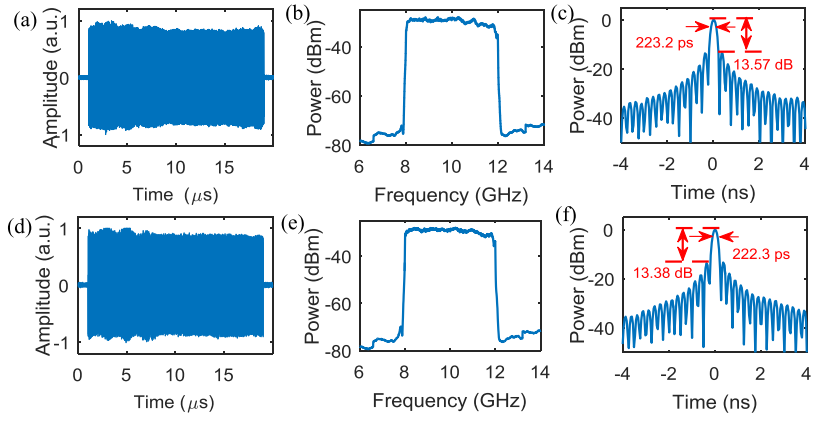

Fig. 3. The LFMW generated at unit radar 1. (a) Waveform, (b) spectrum, (c) de-chirp result. The LFMW generated at unit radar 2. (d) Waveform, (e) spectrum, (f) de-chirp result.

the case where the echo wave power is gradually becoming weak, the echo wave from the target is firstly attenuated by the variable microwave attenuator (Atten), then amplified by the EA, and filtered by the BPF. Next, the echo wave is injected into the coherent de-chirp receiver, and the de-chirp processes are implemented by sending the output optical signals of MZM2/MZM4 into PD3/PD4, separately. The IF signals are amplified, low-pass filtered, and finally sent to the digital signal oscilloscope (DSO81204B, sampling rate 100 MSa/s) which performs as the ADC and realize digitalization of the IF signals.

Waveform and spectrum results of the 8–12 GHz LFMW generated at unit radar 1 are shown in Figs. 3(a)–(b). To evaluate the performance of the de-chirp receiver, the generated LFMW is firstly attenuated by 40 dB by attenuator 1 and then sent to the de-chirp receiver. Figure 3(c) shows the spectrum of the de-chirped signal, the peak sidelobe ratio (PSLR) and the full-width at half maximum (FWHM) of the main lobe are 13.57 dB and 223.2 ps, respectively. While Figs. 3(d)–(f)

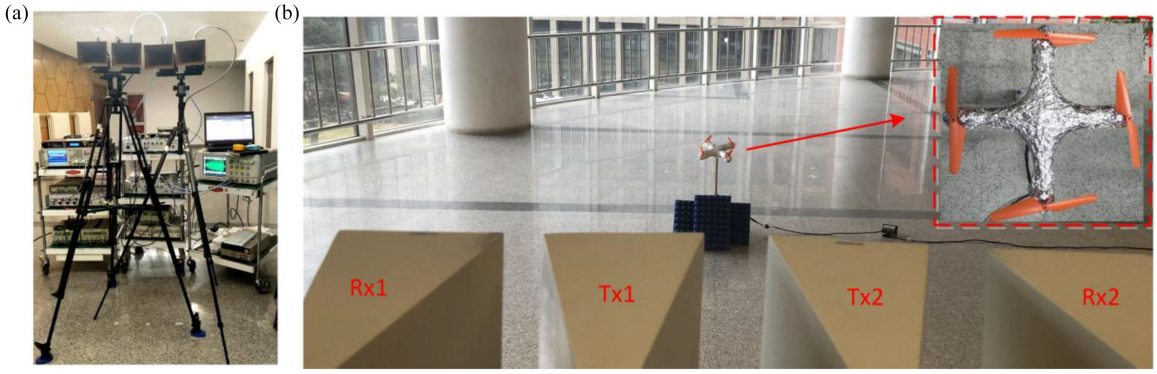

Fig. 4. The photograph of the experimental scene. (a) The photograph of the radar transceiver; (b) the photograph of the antennas and the target.

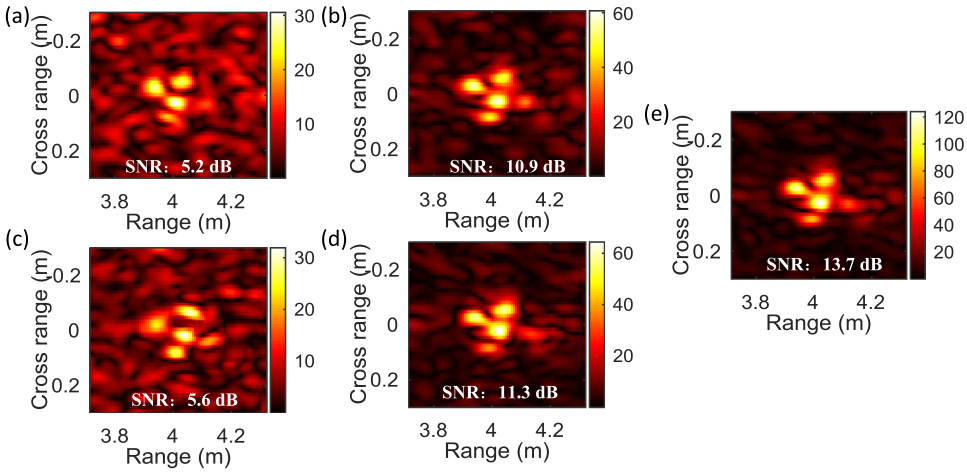

Fig. 5. The ISAR imaging results of the UAV when the attenuation is 39 dB. (a) Monostatic mode; and (b) transmit-coherence mode of radar 1. (c) Monostatic mode; and (d) transmit-coherence mode of radar 2. (e) Full-coherence mode.

show the corresponding results of unit radar 2. The PSLR and FWHM are 13.38 dB and 222.3 ps, separately. The above measured results accord well with the ideal results of 13.32 dB and 221.5 ps, and the FWHM also implies a range resolution of about 3.4 cm.

Then, to assess the system's ability of high-precision imaging for dim-small targets, the ISAR coherent imaging is conducted. Figure 4 shows the experimental scene. At each unit radar, an antenna pair (20 dBi) is used as the transmit and receive antenna, and the baseline between two radars is 0.25 m. A turntable whose rotation speed is 720 degree per second is placed about 4 m away from the antenna pairs, and a small unmanned aerial vehicle (UAV: 0.3 m $\times$ 0.3 m) is placed on the turntable. For the sake of high cross-range resolution, the echo waves after the de-chirp process are sampled for 28 ms, which includes 1400 pulses.

Firstly, the attenuations of attenuator 1 and attenuator 2 are both set to be 39 dB. The ISAR imaging results of the UAV are shown in Fig. 5. Figures 5(a) and (c) show the images obtained by radar 1 and radar 2 in monostatic mode, and Figs. 5(b) and (d) are obtained in transmit-coherence mode. By coherently superimposing the image data in Figs. 5(b) and (d), we acquire the image in full-coherence mode, as shown in Fig. 5(e). From the results, we can see that the complete ISAR image can all be obtained in monostatic, transmit-coherence and full-coherence mode. The SNRs of the images are also calculated according to [24], which is the ratio between the aver-

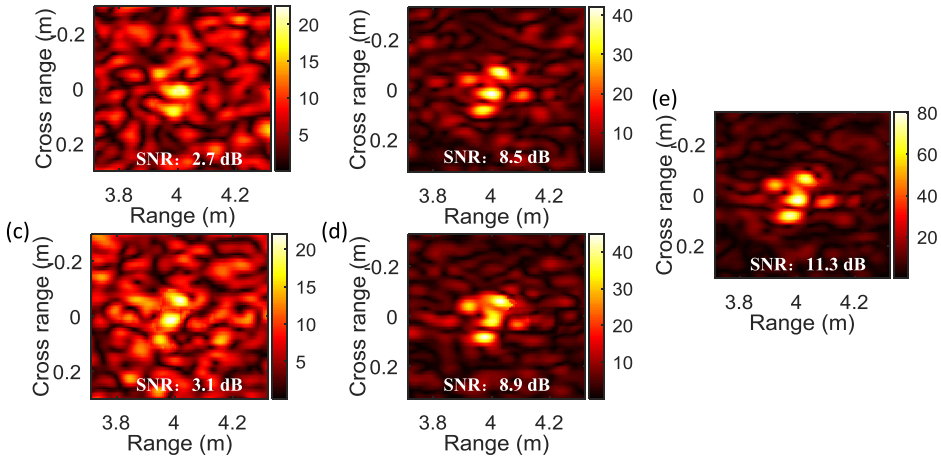

Fig. 6. The ISAR imaging results of the UAV when the echo wave is further reduced by 3 dB. (a) Monostatic mode; and (b) transmit-coherence mode of radar 1. (c) Monostatic mode; and (d) transmit-coherence mode of radar2. (e) Full-coherence mode.

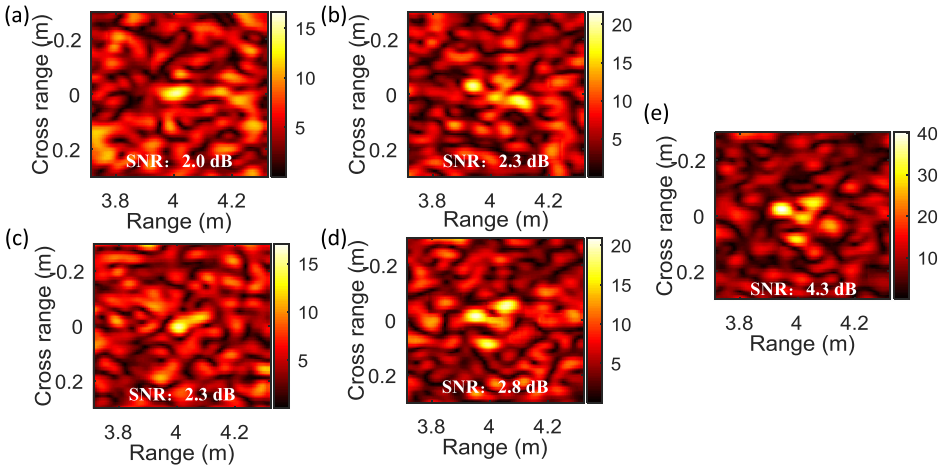

Fig. 7. The ISAR imaging results of the UAV when the echo wave is further reduced by 7 dB. (a) Monostatic mode; and (b) transmit-coherence mode of radar 1. (c) Monostatic mode; and (d) transmit-coherence mode of radar2. (e) Full-coherence mode.

age pixel energy of the target and the background noise. The image SNRs are 5.2 dB and 5.6 dB for radar 1 and radar 2 in monostatic mode, 10.9 dB and 11.3 dB in transmit- coherence mode, and 13.7 dB in full-coherence mode. Compared to the monostatic mode, the image SNR gains in transmit-coherent mode are both 5.7 dB for two unit radars, separately. And when full-coherence is achieved, the image SNRs gains are further improved to 8.5 dB and 8.1 dB, separately. Such SNR gains will improve the imaging and identification precision.

Then the echo wave is further reduced by 3 dB, and the ISAR imaging results are shown in Fig. 6. The image SNRs are 2.7 dB and 3.1 dB for radar 1 and radar 2 in monostatic mode, 8.5 dB and 8.9 dB in transmit- coherence mode, and 11.3 dB in full-coherence mode. In monostatic mode when only one radar works, parts of the UAV are below the noise level, and it's hard to recognize that the target is a UAV. While in transmit-coherence mode and full-coherence mode, due to the SNR gain, the whole UAV image is above the noise floor and the UAV can be clearly seen.

After that, the echo wave is further reduced by 7 dB, and the imaging results are shown in Fig. 7. The image SNRs are 2.0 dB and 2.3 dB for radar 1 and radar 2 in monostatic mode, 2.3 dB and

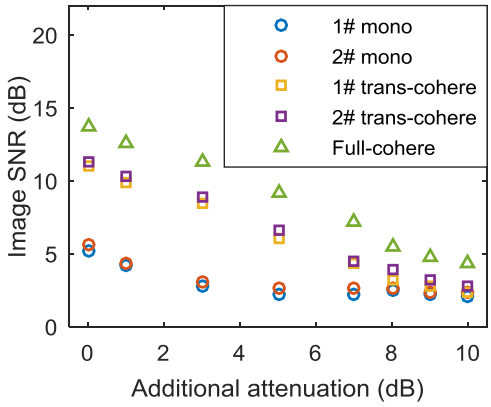

Fig. 8. The image SNRs when the additional attenuation is from 0 dB to 10 dB. 1# (2#) mono: radar 1 (radar 2) works in monostatic mode; 1# (2#) trans-cohere: radar 1 (radar 2) works in transmit-coherence mode. Full-cohere: full-coherence mode.

2.8 dB in transmit- coherence mode, and 4.3 dB in full-coherence mode. Even in transmit-coherence mode, parts of the UAV are submerged in noise and the UAV cannot be recognized. While when full-coherence is achieved, the complete UAV image is obtained.

The image SNRs when the echo power is gradually attenuated from 39 dB to 49 dB are also shown in Fig. 8, and the horizontal axis represents the additional attenuation on the basis of 39 dB. When the additional attenuation is from 0 dB to 3 dB, the image SNRs in all three modes gradually degrades. And the image SNRs in transmit-coherence mode and full-coherence mode are above 5.7 dB and 8.1 dB higher than those in monostatic mode, respectively. When the additional attenuation is increased to above 3 dB, the SNRs in monostatic mode fluctuates because the scatters of the UAV submerge below the noise floor, while the image SNRs in transmit-coherence and full-coherence mode still decrease as the echo power becomes weaker. And the image SNRs in full-coherence mode are above 1.5 dB higher than that in transmit-coherence mode. Due to the above SNR gains, when the echo wave becomes increasingly weaker and image of the UAV cannot be seen in monostatic mode, it can still be clearly seen through transmit-coherence mode and full-coherence mode. While when the UAV cannot be identified in transmit-coherence mode, it can still be recognized when full-coherence is realized, capitalizing on the further SNR gain. In other words, compared to the single radar, the DCAR improves the SNR, and makes it easier to image and identify dim-small targets.

The above results also show that the obtained image SNR gain is a little bit different from the theoretical value. According to the operation principle, a theoretical SNR gain of N^3 can be obtained in full-coherence mode when N identical transceivers are applied. In our real system, as the performance of two transceivers are not perfectly consistent with each other, the obtained image SNR gain is a bit lower than the theoretical value. In addition, when the target has multiple scattering points, one of the scattering points is chosen as the main scattering point and the ideal coherent synthesis can be realized at this point. While for other scattering points, as the time delay settings are not ideal for them, the SNR gain will be degraded.

4. Conclusion

A photonics-assisted broadband DCAR for high-precision imaging of dim-small targets is put forward. The ISAR coherent imaging for a small UAV (0.3 m $\times$ 0.3 m) is experimentally implemented by a two-unit X-band DCAR, and the range and cross range resolution are $\sim$3.4 cm and $\sim$3.6 cm, separately. When full-coherence is realized, about 8.5 dB image SNR gain can be obtained compared to that when only one unit radar works. Due to the SNR gain, the DCAR is capable to obtain the complete images of the weaker targets and identify them. The results reveal that the proposed

photonics-assisted broadband DCAR has the capability of high-precision imaging and identification for dim-small targets.

References

[1] X. Chen, J. Guan, Y. He, and J. Zhang, "Detection of low observable moving target in sea clutter via fractal characteristics in fractional Fourier transform domain," *IET Radar Sonar Navigat.*, vol. 7, no. 6, pp. 635–651, 2013.

[2] C. Shi, D. Luo, and X. Deng, "Dynamic programming algorithm for the detection of air dim target," in *Proc. IET Int. Radar Conf.*, 2013, pp. 1–3.

[3] S. Zhu, G. Liao, D. Yang, and H. Tao, "A new method for radar high-speed maneuvering weak target detection and imaging," *IEEE Geosci. Remote Sens. Lett.*, vol. 11, no. 7, pp. 1175–1179, Jul. 2014.

[4] X. Chen, Y. Huang, N. Liu, J. Guan, and Y. He, "Radon-fractional ambiguity function-based detection method of low-observable maneuvering target," *IEEE Trans. Aerosp. Electron. Syst.*, vol. 51, no. 2, pp. 815–833, Apr. 2015.

[5] M. I. Skolnik, *Introduction to Radar Systems*. New York, NY, USA: McGraw-Hill, 2001.

[6] X. Wang, W. Song, Z. Zhang, and H. Zhu, "A TBD algorithm based on dynamic-programming for dim radar target detection," in *Proc. IEEE 10th Int. Conf. Signal Process.*, 2010, pp. 2133–2136.

[7] K. M. Cuomo, S. D. Coutts, J. C. McHarg, N. B. Pulsone, and F. C. Robey, "Wideband aperture coherence processing for next generation radar (NexGen)," Lexington, MA, USA: MIT Lincoln Lab. Tech. Rep. ESC-TR-2004-087, 2004.

[8] S. Coutts, K. Cuomo, J. McHarg, F. Robey, and D. Weikle, "Distributed coherent aperture measurements for next generation BMD radar," in *Proc. 4th IEEE Workshop Sensor Array Multichannel Process.*, 2006, pp. 390–393.

[9] H. Gao, Z. Cao, S. Wen, and Y. Lu, "Study on distributed aperture coherence-synthesizing radar with several experiment results," in *Proc. IET Int. Radar Conf.*, 2011, pp. 84–86.

[10] H. Gao, Z. Cao, Y. Lu, and P. Wang, "Development of distributed aperture coherence-synthetic radar technology," in *Proc. IET Int. Radar Conf.*, 2013, pp. 1–6.

[11] P. Yin, T. Zeng, and Q. Liu, "Wideband distributed coherent aperture radar based on stepped frequency signal: Theory and experimental results," *IET Radar Sonar Navigat.*, vol. 10, no. 4, pp. 672–688, 2016.

[12] R. H. Walden, "Analog-to-digital conversion in the early twenty-first century," in *Wiley Encylopedia of Computer Science and Engineering, Benjamin* W. Wah ed. Hoboken, NJ, USA: Wiley, 2008.

[13] J. Vankka and K. A. I. Halonen, "*Direct Digital Synthesizers: Theory, Design, and Applications*," Espoo, Finland: Helsinki University of Technology, 2001.

[14] J. Yao, "Microwave photonics," *J. Lightw. Technol.*, vol. 27, no. 3, pp. 314–335, Feb. 2009.

[15] J. Capmany and D. Novak, "Microwave photonics combines two worlds," *Nature Photon.*, vol. 1, no. 6, pp. 319–330, 2007.

[16] X. Xiao *et al.*, "A microwave photonics-based inverse synthetic aperture radar system," in *Proc. Conf. Lasers Electro-Opt.*, 2017, pp. 1–2.

[17] F. Zhang *et al.*, "Photonics-based broadband radar for high-resolution and real-time inverse synthetic aperture imaging," *Opt. Exp.*, vol. 25, no. 14, pp. 16274–16281, 2017.

[18] R. Li *et al.*, "Demonstration of a microwave photonic synthetic aperture radar based on photonic-assisted signal generation and stretch processing," *Opt. Exp.*, vol. 25, no. 13, pp. 14334–14340, 2017.

[19] S. Peng *et al.*, "High-resolution W-band ISAR imaging system utilizing a logic-operation-based photonic digital-to-analog converter," *Opt. Exp.*, vol. 26, no. 2, pp. 1978–1987, 2018.

[20] A. Wang *et al.*, "Ka-band microwave photonic ultra-wideband imaging radar for capturing quantitative target information," *Opt. Exp.*, vol. 26, no. 16, pp. 20708–20717, 2018.

[21] X. Xiao *et al.*, "Photonics-based wideband distributed coherent aperture radar system," *Opt. Exp.*, vol. 26, no. 26, pp. 33783–33796, 2018.

[22] K. B. Cooper, R. J. Dengler, N. Llombart, B. Thomas, G. Chattopadhyay, and P. H. Siegel, "THz imaging radar for standoff personnel screening," *IEEE Trans. Terahertz Sci. Technol.* Vol. 1, no. 1, pp. 169–182, Sep. 2011.

[23] J. Liao *et al.*, "Novel photonic radio-frequency arbitrary waveform generation based on photonic digital-to-analog conversion with pulse carving," in *Proc. Conf. Lasers Electro-Opt.*, 2015, pp. 1–2.

[24] R. D. Fiete and T. Tantalo, "Comparison of SNR image quality metrics for remote sensing systems," *Opt. Eng.*, vol. 40, no. 4, pp. 574–585, 2001.